HAL open science

Impact of spatial harmonic waves on dielectric particles displacement in standing and traveling wave electric fields

Ayyoub Zouaghi, Noureddine Zouzou

▶ To cite this version:

Ayyoub Zouaghi, Noureddine Zouzou. Impact of spatial harmonic waves on dielectric particles displacement in standing and traveling wave electric fields. Journal of Electrostatics, 2019, 98, pp.25-33. 10.1016/j.elstat.2019.01.006 . hal-02446755

HAL Id: hal-02446755

https://hal.science/hal-02446755v1

Submitted on 21 Oct 2021

HAL is a multi-disciplinary open access archive for the deposit and dissemination of scientific research documents, whether they are published or not. The documents may come from teaching and research institutions in France or abroad, or from public or private research centers.

L'archive ouverte pluridisciplinaire **HAL**, est destinée au dépôt et à la diffusion de documents scientifiques de niveau recherche, publiés ou non, émanant des établissements d'enseignement et de recherche français ou étrangers, des laboratoires publics ou privés.

Distributed under a Creative Commons Attribution - NonCommercial 4.0 International License

Version of Record: https://www.sciencedirect.com/science/article/pii/S0304388618303413
Manuscript_8df4d72431f0a91fed6bff14fb96b62e

Impact of Spatial Harmonic Waves on Dielectric Particles Displacement in Standing and Traveling Wave Electric Fields

Ayyoub Zouaghi* and **Noureddine Zouzou**

Institut PPRIME

CNRS, Université de Poitiers, ISAE-ENSMA

F-86962 Futuroscope Chasseneuil, France

*Corresponding author: ayyoub.zouaghi@univ-poitiers.fr

ABSTRACT

The purpose of this work is to investigate the effect of spatial harmonic waves on dielectric particles displacement process using standing and traveling electric wave electric conveyors. This investigation is divided into two main parts. The first one is an experimental study, where the efficiency of conveyors for the displacement of micrometer sized PMMA particles is analyzed. The second part consists of a numerical and theoretical study in which the spatial electric potential distribution and the consequences on the spatial harmonics on particles displacement is investigated. The results show that the displacement efficiency and the particles direction depend basically on the particles size, the charge to mass ratio, the applied voltage and the frequency. In the standing wave conveyor, the particles move toward both right and left directions. In the traveling wave conveyor, at high voltage, low frequency, small particles or high charge to mass ratio conditions particles move toward the traveling wave direction. In the case of low applied voltage, high frequency or if the particles have a low charge to mass ratio, some particles move toward the opposite direction because of the backward harmonic wave that appears near to the surface. The magnitude of the harmonic waves depends on the levitation height of particles; it can be controlled by varying the number of phases, the gap spacing or the thickness of electrodes or by adding a dielectric barrier over the surface.

KEYWORDS: traveling wave, standing wave, electric potential, dielectric particles, spatial harmonics, fast Fourier transform

© 2019 published by Elsevier. This manuscript is made available under the CC BY NC user license
https://creativecommons.org/licenses/by-nc/4.0/

1. INTRODUCTION

The use of non-uniform electric field for dielectric particles monitoring, sampling, classification and displacement is getting more attention in different research and industrial domains [1–5]. In fact, the mechanical processes used actually have many issues, they are expensive, energy consuming and less flexible; thought, developing new techniques that exhibit electrostatic forces can offer a more efficient alternative. One of the promising electrostatic devices is the so-called the electric curtain. It is composed of a series of parallel electrodes deposited on a dielectric surface and energized by a multiphase electric potential [6–10]. In this system, if the electric field is high enough, Coulomb force can overcome the attractive forces such as gravitational force, image force and adhesion force, and leads to the particles motion [6–10].

Masuda was one of the first researchers who developed and studied this system. He conducted a series of both experimental and theoretical studies to investigate the particles behavior in the seventies and eighties of the last century [6,7]. Masuda was the first one who highlighted the effect of spatial harmonics on the particles trajectory in a 3-phase system. Based on his works, Melcher et al. [11,12] conducted more extensive theoretical studies using 6-phase high voltage system. They focused on the different modes of motion of particles as a function of frequency. They reported that the particles may be transported in different modes as a function of frequency. The same interpretations were given by Balachandran et al. based on a different model [13,14].

One of the first applications of this system was in the domain of electrophotography for toner supply in the printers [15,16]. After then, lot of research groups used the principle of the electric curtain in microships for biological applications [17]. In dielectric liquid medium, the dielectrophoretic force becomes strong enough to move particles and species [18]. Dipole force doesn’t depend on the particle charge, rather than, it depends on the size and the dielectric characteristics of the particle and the medium in which it is emerged; it depends also on the gradient of the electric field [18]. In the last fifteen years, thanks to the development of thin films deposition

technology that allow us to deposit transparent electrodes on transparent substrate; a lot of research groups have been interested on using the technique of the electric curtain to develop the so called Electrodynamic Screen (EDS) [19–23]. This system is used for dust removal from photovoltaic panels and solar collectors. In fact, the accumulation of dust and sand on the photovoltaic systems can highly reduce their efficiency; the traditional systems such as washing and brushing consume a huge quantity of water and energy and damage the PV collectors. The works carried out by Muzumder et al. [19–23], Calle et al. [24–26] and Kawamoto at al. [27–30] in this field showed promising results in both terrestrial and extraterrestrial conditions.

Manipulating powdery dielectric materials is a common process in many industries such as recycling [31]. The effect of forces such as Coulomb force, dielectrophoretic force, image force, adhesion force, drag force and gravity, on the particles motion has been studied extensively in many research works [8,10,20]. Studing the forces balance is indispensable to determine the motion of particles; however, a more detailed study of spatio-temporal distribution of the electric potential is necessary for a more complete understanding of some particles behaviors experimentally observed such as the direction of particles movement. The purpose of this work is to investigate the particles displacement efficiency, not only in the case of traveling wave multiphase conveyor (TWC), but also on the standing wave 2-phase electric conveyor (SWC). In this study we are focusing on the effect of the electric potential harmonic waves on the particles displacement process using such device; the influence of the experimental parameters on the harmonic waves is also part of this study. This investigation is composed of two parts. The first part is an experimental study where we analyze the efficiency of conveyors for the displacement of micrometer sized PMMA particles. The effects of frequency, applied voltage value, particle size and charge to mass ratio are investigated. A comparative study between the two conveyors has been also carried out. The second part consists of a numerical and theoretical study in which the electric potential distribution and the effect of the harmonic waves on particles behavior is investigated. The results of the theoretical study are used to

understand and explain the experimental observations. The effect of different parameters such as the number of the potential phases, and the presence of dielectric barrier on the waves magnitude is also carried out.

2. EXPERIMENTAL SETUP AND PROTOCOL

The objective of this experimental study is to evaluate the efficiency of the conveyors for dielectric particles displacement. The experimental setup (case of SWC) used here is represented schematically in Figure 1.

The experimental protocol is as follows: for each measuring point, a mass of 5 g of calibrated spherical PMMA particles is deposited at the end of a vibrating particles supply system. Once the system is turned on, the particles move throughout the vibrating plate and fall on the electrostatic conveyor. During this step, the particles can acquire an initial electrostatic charge by friction with the metallic plate as well as by inter-particle collisions. This initial charge is necessary for starting the movement under the electric field. When the particles arrive on the conveyor, they move in both x-directions and fall into two Faraday cups made of stainless steel. The two buckets are connected to electrometers (Keithley Model 6514) to measure the charge. After that, we take measurement of the mass of particles collected in both sides. For each measurement, three mass and charge values are recorded: the initial charge of particles, the mass and the charge of the particles evacuated in the direction of the electric field wave (right or forward direction), the mass and the charge of those evacuated in the opposite direction of the electric field wave (left or backward direction) and finally the mass of the particles remaining on the conveyor. Each measurement point is repeated three times; the mean and the standard deviation are calculated. The particles evacuation efficiency is calculated using this formula:

$$Eff(\%) = \frac{m_{disp}}{m_{tot}} \times 100 \quad (1)$$

where, m_{disp} the mass of the evacuated particles, it is equivalent to the sum of the two masses recovered on the two Faraday cups in both sides. m_{tot} is the total mass equal to the sum of the mass of displaced particles and the mass of non-displaced particles that remain on the conveyor. The experiments were carried out at room temperature ($25° \pm 2°$) and a relative humidity between 40 and 50 %.

The multiphase applied high voltage (HV) waveforms are supplied by multiple high voltage power amplifiers (Trek, model 2220, $\pm 2\ kV$, $\pm 20\ \mu A$) controlled by a digital function generator (TTi, TGA1240, 16 MHz). A digital pulse generator (Stanford, model DG645) is used as a synchronizer for triggering the three electrical signals supplied to the conveyor. The whole system can provide 2 or 4-phase sinusoidal high voltage signals with an amplitude up to 2 kV and a frequency up to 10 kHz. The signals are visualized using a digital oscilloscope (Lecroy 424, 200 MHz, 2 GS/s).

2.1. Conveyors conception

Figure 2 represents a cross-sectional view in $x - y$ plan of the standing and traveling wave configurations. Both of the conveyors are composed of several copper electrodes of 1 mm in width and 35 μm in thickness, deposited in parallel on a dielectric surface of $10 \times 10\ cm^2$. The dielectric surface is made of epoxy resin reinforced with fiberglass ($\varepsilon_r = 4.3$). The gap spacing between the electrodes is fixed at 1 mm, which makes the geometrical periodicity $\lambda = 4\ mm$ in the case of SWC and $\lambda = 8\ mm$ in the case of TWC. In our experiments, we limited the applied voltage value at 1 kV in 2-phase configuration and 1.4 kV in 4-phase configuration in order to prevent the appearance of corona discharges near electrode edges. Since there is no electrical discharge, the particles can only be charged by triboelectric mechanism caused by particle-surface and particle-particle collisions.

2.2. Particles characterization

The particles under investigation are made of PMMA dielectric material and have a spherical shape. Figure 3 illustrates a microscope image of the used particles and their size ranges after classification. The particles are classified using an automatic sieving device (Endecotts, model Octagon 200) into five classes having a median particles diameter of 56.8, 120, 143, 196 and $260\ \mu m$, respectively. The particles size distribution is measured using Malvern laser particle size analyser (Mastersizer 3000). We can see that their size is ranging between some tens to hundreds of micrometers. The particles diameter ranges of the different classes are mentioned in Table 1.

Table 1. Particles size range characteristics.

Class	$dp(10)$ [µm]	$dp(50)$ [µm]	$dp(90)$ [µm]
1	36.5	56.8	86.4
2	80.5	120	173
3	98.4	143	198
4	134	196	277
5	162	260	399

3. RESULTS AND DISCUSSION

In this section, we investigate experimentally the effect of several parameters such as the particle size and charge, the applied voltage value, and the frequency on the particles displacement efficiency.

3.1. Influence of the particle size

The influence of the particles size on the displacement efficiency of both standing and traveling wave conveyors is illustrated in Figure 4. In this experiment, five different particles size ranges are investigated. The applied voltage and frequency are set at $1\ kV$ and $50\ Hz$, respectively. In both configurations, we see that when particle size increases, the displacement efficiency decreases. This can be explained by the fact that big particles are heavier, so the gravitational attractive force value

becomes higher than the electric repulsive force, which is the responsible of particles motion. The contribution of the electric force can be improved either by increasing the applied electric field or by increasing the particles charge. For all the particles size ranges, the total displacement efficiency is higher in the case of TWC, reaching 100 % for the particles from the first size class.

In the case of SWC, we notice that the particles are moved toward both right and left sides. The quantity of particles in both sides is nearly the same. This result was expected because of the symmetrical 2-phase configuration. In the other hand, in the case of TWC, most of particles move to the forward direction of the electric wave. We can see also that there is a small quantity of particles moving backward. Their quantity increases with the particles size. This phenomena has been observed and analyzed by other authors, such as Masuda et al. [6,7], and Balachandran et al. [13,14] but under different experimental conditions and with different type of particles. Based on their research works, the displacement of particles to the opposite direction is explained by the fact that the non-sinusoidal space distribution of electric potential over the surface create some harmonic waves that propagate backward as a function of time. The next section is dedicated to the analysis of the electric potential waves using numerical simulation in order to understand the experimental results.

3.2. Particles charge

The effect of particles size on the charge to mass ratio is also investigated in this section. The results are illustrated in Figure 5 for both standing and traveling wave configurations. As mentioned before, the particles acquire their charge through triboelectric mechanism by friction or contact with each other and with the metallic vibrating feeder. For the five size ranges studied in this paper, most of the particles are positively charged and the charge per gram is of the order of a few tens of nC/g. In the case of SWC, we can see that the moved particles have higher charge than the particles that remain on the surface. We notice also that the particles moved toward the left and the right directions have nearly the same charge to masse ratio.

In the case of TWC, the particles that have a high charge to mass ratio are moved forward by the electric wave, and the particles that have a lower charge to mass ratio are moved backward. The particles that have very low charge to mass ratio are not moved (they remain on the surface). This is because the Coulomb force is not strong enough to initiate their motion in a specific direction.

3.3. Influence of the applied voltage value

Figure 6 illustrates the influence of the applied voltage value on particles displacement efficiency in both standing and traveling wave configurations. The particles used in this experiment are from the third class, and the frequency is fixed at $50\ Hz$. As expected, increasing the applied voltage value improves the particles displacement efficiency because of the contribution the Coulomb's force. We mention also that we can increase the applied voltage till reach $1400\ V$ in the case of 4-phase configuration before corona discharge appearance. However, corona discharge ignites at lower applied voltage in the case of 2-phase configuration. This is because the difference of potential between two successive electrodes is higher in the case of 2-phase configuration. It can be seen also that when we decrease the applied voltage in the case of 4-phase configuration, more particles move backward.

3.4. Influence of the frequency

The evolution of the displacement efficiency of the two systems as a function of the frequency is illustrated in Figure 7. The particles used in this experiment are belong to the third class $dp(50) = 143\ \mu m$, and the high voltage magnitude is fixed at $1\ kV$. For both SWC and TWC, the total displacement efficiency increases with the frequency, then passes by a maximum (more than $35\ \%$ with SWC at $50\ Hz$ and 70% with TWC at $20\ Hz$), before a significant decrease at higher frequencies. In a previous works [9,10], we demonstrated using particles visualization techniques that the particles behaves differently as a function of frequency. At low frequency, the particles follow the variation of the alternative electric field, but this phenomenon is too slow. At high

frequencies, the particles cannot follow the fast variation of the electric field, so they just jump and vibrate at small height over the surface.

In the case of SWC, the particles move toward both right and left directions. However, the direction of the particles motion depends on the frequency in the case of TWC. At low frequency, we can see that almost all the particles are moved forward. For frequencies over $50\ Hz$, we notice that there is a considerable mass of particles moving backward. This can be also related to the harmonic waves that appear near the surface. This point will be discussed in detail in the next session.

4. THEORETICAL AND NUMERICAL STUDY

The objective of this part is to study the electric potential harmonic waves in order to understand their impact on the particles displacement.

4.1. Electric potential analysis

Figure 8 illustrates the typical 2D distribution of the electric potential in the space over the electrodes at the moment $t = 0\ s$ for the two conveyors. The electric potential values at the electrodes are 1 and $-1\ kV$ in the case of SWC and $1,\ 0,\ -1,\ 0\ kV$ in the case of TWC. This simulation has been carried out using Finite Element Method (FEM) commercial software by the resolution of Laplace equation. In this simulation, the boundary conditions on the electrodes are given by the Dirichlet conditions, the symmetrical boundaries are given by Neumann conditions and the space charge density is neglected. The results are represented over four consecutive electrodes. The magnitude of the computed potential is indicated by scale color bars on the right sides of the figures. By employing Fast Fourier Transform (FFT) using a Matlab® script, the waveform of electric potential $V(x)$ for a given y-position can be decomposed into multiple harmonics.

Figure 9 represents the ten first Fourier transform coefficients for $y = 0.1\ mm$ over the surface in the case of 2 and 4-phase configurations. In the case of 2-phase SWC, the first harmonic value is

very high compared to the others. The coefficient value of the first harmonic is 0.925, the other harmonics values are less than 5 % compared to the first one. So the effect of harmonics having an order higher than $n = 1$ can be neglected. In the case of 4-phase TWC, the strongest harmonics are the fundamental (0.749) and the third harmonic (0.201); the other harmonic's values are very weak so their effect can be neglected. Those harmonics are due to the deformation of the electric potential caused by the rectangular shape of the electrodes. In fact, the electric potential waveform far from the surface is nearly sinusoidal; however, it is deformed near to the surface because of the rectangular shape of the electrodes. This deformation is responsible of the appearance of spatial harmonics.

Following the same theoretical analysis developed by Masuda et al. [7] for the 3-phase configuration, we can extract the equations of harmonic waves. In the case of 2-phase configuration, by taking only the first harmonic in consideration, the electric potential in the space over the electrodes can be expressed as follows:

$$V(x,y,t) \approx V_0 \left[K_1 e^{-\frac{2\pi}{\lambda}y} \cos\left(\frac{2\pi}{\lambda}x\right) \cos(\omega t)\right] \tag{2}$$

Where, V_0 is the amplitude of the applied voltage waveforms. $\lambda = 4\,mm$ is the potential wavelength in 2-phase configuration. K_1 is the first Fourier transform coefficient. The last expression can be written in this form:

$$V(x,y,t) = V_0 \left[\frac{1}{2}K_1 e^{-\frac{2\pi}{\lambda}y} \cos\left(\frac{2\pi}{\lambda}x - \omega t\right) + \frac{1}{2}K_1 e^{-\frac{2\pi}{\lambda}y} \cos\left(\frac{2\pi}{\lambda}x + \omega t\right)\right] \tag{3}$$

Thus, the standing wave of electric potential can be expressed as the sum of two waves that have the same amplitude and propagate toward opposite directions as a function of time:

$$V(x,y,t) = W_R + W_L = A(y).\cos\left(\frac{2\pi}{\lambda}x - \omega t\right) + A(y).\cos\left(\frac{2\pi}{\lambda}x + \omega t\right) \tag{4}$$

With, $A(y) = \frac{1}{2}V_0.K_1 e^{-\frac{2\pi}{\lambda}y}$ (5)

In the case of 4-phases configuration, taking into account the first and the third harmonics and by following the same reasoning, we find this expression of the applied voltage:

$$V(x,y,t) \approx V_0 \left[K_1 e^{-\frac{2\pi}{\lambda}y} \cos\left(\frac{2\pi}{\lambda}x - \omega t\right) + K_3 e^{-\frac{6\pi}{\lambda}y} \cos\left(\frac{6\pi}{\lambda}x + \omega t\right)\right] \quad (6)$$

In 4-phase configuration, the potential wavelength is $\lambda = 8\,mm$. K_1 and K_3 are the first and the third Fourier coefficients, respectively. We can notice that the traveling wave of electric potential is the sum of two waves of the same frequency propagating in opposite directions:

$$V(x,y,t) \approx W_F + W_B = A_F(y).\cos\left(\frac{2\pi}{\lambda}x - \omega t\right) + A_B(y).\cos\left(\frac{6\pi}{\lambda}x + \omega t\right) \quad (7)$$

With, $\begin{cases} A_F(y) = V_0.K_1 e^{-\frac{2\pi}{\lambda}y} \\ A_B(y) = V_0.K_3 e^{-\frac{6\pi}{\lambda}y} \end{cases}$ (8)

A_F and A_B are the amplitudes of the forward and the backward harmonic waves of the electric potential at a given height y. The two waves W_F and W_B correspond to the first and the third harmonics, respectively.

Figure 10 represents the spatial electric potential waveforms as a function of x position for $y = 0.1\,mm$ and $t = 0$, $T/6$ and $T/4$. The figure illustrates the electric potential waveform obtained by FEM numerical simulation (black line), and the electric potential waveform given by Equations 4 and 7 for SWC and TWC respectively (red line), which is the sum of two electric potential waves W_F and W_B (green and blue lines respectively). As a function of time, the two waves propagate in opposite directions. They have the same amplitude and frequency in the case of SWC. However, the amplitude of the wave that moves forward is higher than the one moving backward. This result is in agreement with the experimental results discussed previously. In TWC, we found that most of particles are moved forward but a small quantity is moved backward because of the second wave. One can observe that the electric potential distribution obtained theoretically by considering only the most important harmonics is close to that obtained by FEM simulation.

4.2. Harmonic waves analysis

In this section, we analyze the spatial harmonics intensity as a function of different parameters such as particle levitation height, electrode width to gap spacing ratio, the number of applied voltage phase and the dielectric barrier permittivity in the case of TWC. This study is important because it allows the optimization of the conveyor configuration by minimizing the backward wave magnitude compared to the forward wave.

Figure 11 illustrates the effect of the levitation height of the particle on the forward and backward harmonic wave amplitudes and the ratio between them. It appears that the magnitude of both harmonics decreases by moving away from the surface. However, the ratio between the amplitudes of the two waves decreases. For instance, $A_B/A_F \approx 25\,\%$ for $h = 0\,mm$ and about $4\,\%$ for $h = 1.2\,mm$. That means that when we go farther from the surface, the impact of the backward harmonic wave, which is responsible for transporting particles to the opposite direction, becomes more negligible compared to the first one. Consequently, the levitation height of the particle has a direct effect on the direction of their movement. Close to the surface, the particles are subjected to the second opposite wave, so they are more likely to be moved backward.

Since Coulomb's force is responsible of particles motion, the levitation height increases with the applied electric field and the particles charge, it increases also with the decrease of the particles size because of the contribution of gravity. In a previous work [9], it has been observed using fast visualization that the particles levitation height decreases also when the frequency increases. In the case of low frequency, high applied voltage, high charge and small size of particles, the particles jump higher where the effect of the backward wave is negligible, so they follow the forward wave. In the other hand, for high frequency, low applied voltage, low charge and big size of particles, the particles stay close to the surface, so some of them can be trapped by the backward harmonic wave. This explanation is in agreement with the experimental results (Figures 4, 5 and 6) and confirms the interpretations given by Masuda et al. [6,7] and Balachandran et al. [13,14] in other conditions.

Figure 12 illustrates the effect of the electrode's width to inter-electrode gap ratio on the amplitudes of the two harmonic waves. We notice that both first and second harmonics amplitudes increase when the ratio between the electrode's width and the spacing gap increases. For the studied w/g values, regarding the ratio of the amplitude of the second wave to the first one, it appears that it reaches its lowest value when the gap spacing is four times bigger than the electrode's width ($w/g = 0.25$). Consequently, small w/g values are recommended if we want to decrease the quantity of particles that goes toward the opposite direction.

The amplitude of spatial harmonic waves can also be controlled by increasing the number of the applied voltage phases. Figure 13 illustrates the effect of the number of phases on the amplitude of the spatial harmonics and the ratio between them. It can be seen that when we increase the number of phases, the amplitude of the direct harmonic wave increases and that of the opposite harmonic wave decreases. Therefore, the contribution of the opposite harmonic wave can be reduced by adding more phases of the applied voltage. By increasing the number of phases, the wavelength of the backward wave decreases. One can notice that the opposite wave in the cases of 3, 4, 5, 6, 7, 8-phase configurations corresponds to the harmonics number 2, 3, 4, 5, 6 and 7, respectively.

In this study, we investigated also the effect of the presence of dielectric barrier on the harmonic wave's amplitude. The results obtained are illustrated in Figure 14. The dielectric barrier has a thickness of $100\ \mu m$. The harmonics values are calculated over the surface of the dielectric barrier. It can be seen that the amplitude of both direct and opposite waves increases with the dielectric constant of the dielectric barrier. However, the A_B/A_F ratio varies differently; it increases to reach a value of 28.65 % for $\varepsilon_r = 4$, then it decreases when the dielectric constant of the dielectric barrier increases. For the studied values of ε_r, the lowest value of A_B/A_F is obtained when there is no dielectric barrier (26.7 %), which is not so far from the highest obtained value. Consequently, adding a dielectric barrier material with high dielectric constant increases the A_B/A_F ratio but not

with a considerable value, so we can add a dielectric barrier for more security or to make the surface smoother without affecting too much the magnitude of spatial potential waves.

5. CONCLUSION

In the present paper, we investigated the effect of harmonic waves on dielectric powdery materials displacement using standing and traveling electric waves. The results obtained are summarized as follows:

(1) The displacement efficiency of particles increases with the applied voltage, decreases when the particles size increases because of the gravitational force contribution and passes by a maximum as a function of frequency. The total displacement efficiency is higher in the case of TWC.

(2) In the case of SWC, the particles are moved toward both right and left directions. In the case of TWC, most of particles move toward the forward direction of the electric wave, but there is a small mass of particles move backward because of the contribution of spatial harmonic waves.

(3) The spatial waveform of the electric potential can be expressed as the sum of two main harmonic waves that propagate in opposite directions. Those harmonics appear near to the surface because of the rectangular geometry of electrodes, which causes a deformation in the electric potential wave

(4) In TWC, at low frequency, high applied voltage, small particles or high charge to mass ratio, particles move forward. At high frequency, low applied voltage value, big particles or low charge to mass ratio, particles move close to the surface, so some of them can be trapped by the opposite wave and go backward.

(5) The amplitude of the harmonic waves can be controlled by changing the number of phases, the electrode width or the gap spacing and by adding a dielectric barrier over the electrodes. By adding more phases, the effect of the backward wave can be eliminated.

ACKNOWLEDGEMENTS

This research was supported by the French Ministry of Higher Education, Research and Innovation (M.E.S.R.I.). The authors gratefully acknowledge Prof. Akira Mizuno, Prof. Lucian Dascalescu and Mr. Olivier Negro for their assistance and expertise.

REFERENCES

[1] J.-S. Chang, A.J. Kelly, J.M. Crowley, Handbook of Electrostatic Processes, CRC Press, 1995.

[2] T.B. Jones, Electromechanics of Particles by Thomas B. Jones, 1995. doi:10.1017/CBO9780511574498.

[3] L. Dascalescu, R. Morar, A. Iuga, A. Samuila, V. Neamtu, I. Suarasan, Charging of particulates in the corona field of roll-type electroseparators, J. Phys. Appl. Phys. 27 (1994) 1242. doi:10.1088/0022-3727/27/6/023.

[4] F. Kherbouche, Y. Benmimoun, A. Tilmatine, A. Zouaghi, N. Zouzou, Study of a new electrostatic precipitator with asymmetrical wire-to-cylinder configuration for cement particles collection, J. Electrost. 83 (2016) 7–15. doi:10.1016/j.elstat.2016.07.001.

[5] A. Zouaghi, N. Zouzou, A. Mekhaldi, R. Gouri, Submicron particles trajectory and collection efficiency in a miniature planar DBD-ESP: Theoretical model and experimental validation, J. Electrost. 82 (2016) 38–47. doi:10.1016/j.elstat.2016.05.004.

[6] S. Masuda, K. Fujibayashi, K. Ishida, H. Inaba, Confinement and transportation of charged aerosol clouds via electric curtain, Electr. Eng. Jpn. 92 (1972) 43–52. doi:10.1002/eej.4390920106.

[7] S. Masuda, M. Washizu, M. Iwadare, Separation of Small Particles Suspended in Liquid by Nonuniform Traveling Field, IEEE Trans. Ind. Appl. IA-23 (1987) 474–480. doi:10.1109/TIA.1987.4504934.

[8] H. Kawamoto, K. Seki, N. Kuromiya, Mechanism of travelling-wave transport of particles, J. Phys. Appl. Phys. 39 (2006) 1249. doi:10.1088/0022-3727/39/6/036.

[9] A. Zouaghi, N. Zouzou, L. Dascalescu, Effect of travelling wave electric field on fine particles motion on an electrodynamic board, in: 2017 IEEE Ind. Appl. Soc. Annu. Meet., 2017: pp. 1–6. doi:10.1109/IAS.2017.8101701.

[10] A. Zouaghi, N. Zouzou, L. Dascalescu, Assessment of forces acting on fine particles on a traveling-wave electric field conveyor: Application to powder manipulation, Powder Technol. 343 (2019) 375–382. doi:10.1016/j.powtec.2018.11.065.

[11] J.R. Melcher, E.P. Warren, R.H. Kotwal, Theory for Pure-Traveling-Wave Boundary-Guided Transport of Tribo-Electrified Particles, Part. Sci. Technol. 7 (1989) 1–21. doi:10.1080/02726358908906520.

[12] J.R. Melcher, E.P. Warren, R.H. Kotwal, Traveling-wave delivery of single-component developer, IEEE Trans. Ind. Appl. 25 (1989) 956–961. doi:10.1109/28.41264.

[13] D. Hu, W. Balachandran, W.W. Machowski, Design of traveling-wave field panel for pharmaceutical powders based on computer simulation of particle trajectories, IEEE Trans. Ind. Appl. 33 (1997) 641–650. doi:10.1109/28.585853.

[14] W. Machowski, W. Balachandran, Dispersion and transport of cohesive lactose powder using travelling wave field technique, Powder Technol. 99 (1998) 251–256. doi:10.1016/S0032-5910(98)00118-1.

[15] F.W. Schmidlin, Development apparatus, US4647179A, 1987. https://patents.google.com/patent/US4647179/en (accessed December 7, 2018).

[16] F.W. Schmidlin, A new nonlevitated mode of traveling wave toner transport, IEEE Trans. Ind. Appl. 27 (1991) 480–487. doi:10.1109/28.81831.

[17] A. Ramos, H. Morgan, N.G. Green, A. Castellanos, Ac electrokinetics: a review of forces in microelectrode structures, J. Phys. Appl. Phys. 31 (1998) 2338. doi:10.1088/0022-3727/31/18/021.

[18] H.A. Pohl, Dielectrophoresis: the behavior of neutral matter in nonuniform electric fields, Cambridge University Press, Cambridge; New York, 1978.

[19] M.K. Mazumder, R.A. Sims, J.D. Wilson, Transparent self-cleaning dust shield, US6911593B2, 2005. https://patents.google.com/patent/US6911593B2/en (accessed December 7, 2018).

[20] A. Sayyah, M.N. Horenstein, M.K. Mazumder, G. Ahmadi, Electrostatic force distribution on an electrodynamic screen, J. Electrost. 81 (2016) 24–36. doi:10.1016/j.elstat.2016.02.004.

[21] A. Sayyah, R.S. Eriksen, M.N. Horenstein, M.K. Mazumder, Performance Analysis of Electrodynamic Screens Based on Residual Particle Size Distribution, IEEE J. Photovolt. 7 (2017) 221–229. doi:10.1109/JPHOTOV.2016.2617088.

[22] M.K. Mazumder, R. Sharma, A.S. Biris, J. Zhang, C. Calle, M. Zahn, Self-Cleaning Transparent Dust Shields for Protecting Solar Panels and Other Devices, Part. Sci. Technol. 25 (2007) 5–20. doi:10.1080/02726350601146341.

[23] M.N. Horenstein, M. Mazumder, R.C. Sumner, Predicting particle trajectories on an electrodynamic screen – Theory and experiment, J. Electrost. 71 (2013) 185–188. doi:10.1016/j.elstat.2012.10.005.

[24] C.I.I. Calle, Electrodynamic Dust Shield for Surface Exploration Activities on the Moon and Mars, in: Valencia, Spain, 2006. https://ntrs.nasa.gov/search.jsp?R=20130012545 (accessed December 7, 2018).

[25] C.I. Calle, C.R. Buhler, J.L. McFall, S.J. Snyder, Particle removal by electrostatic and dielectrophoretic forces for dust control during lunar exploration missions, J. Electrost. 67 (2009) 89–92. doi:10.1016/j.elstat.2009.02.012.

[26] C.I. Calle, C.R. Buhler, M.R. Johansen, M.D. Hogue, S.J. Snyder, Active dust control and mitigation technology for lunar and Martian exploration, Acta Astronaut. 69 (2011) 1082–1088. doi:10.1016/j.actaastro.2011.06.010.

[27] H. Kawamoto, Some techniques on electrostatic separation of particle size utilizing electrostatic traveling-wave field, J. Electrost. 66 (2008) 220–228. doi:10.1016/j.elstat.2008.01.002.

[28] H. Kawamoto, M. Uchiyama, B.L. Cooper, D.S. McKay, Mitigation of lunar dust on solar panels and optical elements utilizing electrostatic traveling-wave, J. Electrost. 69 (2011) 370–379. doi:10.1016/j.elstat.2011.04.016.

[29] H. Kawamoto, T. Shibata, Electrostatic cleaning system for removal of sand from solar panels, J. Electrost. 73 (2015) 65–70. doi:10.1016/j.elstat.2014.10.011.

[30] H. Kawamoto, B. Guo, Improvement of an electrostatic cleaning system for removal of dust from solar panels, J. Electrost. 91 (2018) 28–33. doi:10.1016/j.elstat.2017.12.002.

[31] A. Belgacem, A. Tilmatine, Y. Bellebna, F. Miloua, N. Zouzou, L. Dascalescu, Experimental analysis of the transport and the separation of plastic and metal micronized particles using travelling waves conveyor, IEEE Trans. Dielectr. Electr. Insul. 25 (2018) 435–440. doi:10.1109/TDEI.2017.006601.

FIGURES CAPTIONS

Figure 1. Illustration of the experimental setup.

Figure 2. Illustration of the studied configurations (a) 2-phase standing wave configuration (b) 4-phase traveling wave configuration, $w = g = 1\ mm$, $e = 35\ \mu m$, $d' = 1.25\ mm$.

Figure 3. Illustration of spherical PMMA particles size distribution in different classes.

Figure 4. Evolution of the particles displacement efficiency as a function of their size for (a) SWC and (b) TWC. Conditions: $V = 1\ kV$, $f = 50\ Hz$.

Figure 5. Evolution of charge to mass ratio as a function of the particles size for (a) SWC and (b) TWC. Conditions: $V = 1\ kV$, $f = 50\ Hz$.

Figure 6. Evolution of the particles displacement efficiency as a function of the applied voltage value for (a) SWC and (b) TWC. Conditions: $dp(50) = 143\ \mu m$, $f = 50\ Hz$.

Figure 7. Evolution of the particles displacement efficiency as a function of the frequency for (a) SWC and (b) TWC. Conditions: $dp(50) = 143\ \mu m$, $V = 1\ kV$.

Figure 8. 2D illustration of the electric potential distribution. Conditions: $V = 1\ kV$, $f = 50\ Hz$.

Figure 9. Illustration of the 10 first harmonics of the spatial waveform of electric potential above the surface. Conditions: $V_0 = 1\ kV$, $f = 50\ Hz$, $y = 0.1\ mm$.

Figure 10. Spatial waveforms of electric potential and their decomposition to harmonics at the moments $t = 0, \frac{T}{6}$ and $\frac{T}{4}$. (a), (c) and (e) correspond to SWC. (b), (d) and (f) correspond to TWC. Conditions: $V_0 = 1\ kV$, $f = 50\ Hz$, $y = 0.1\ mm$.

Figure 11. Effect of the levitation height on the forward and backward harmonic waves amplitudes. Conditions: $V_0 = 1\ kV$, $f = 50\ Hz$, 4-phase configuration.

Figure 12. Effect of width to gap spacing ratio on the forward and backward harmonic waves amplitudes for $y = 0.1\ mm$. Conditions: $V_0 = 1\ kV$, $f = 50\ Hz$, 4-phase configuration.

Figure 13. Effect of the number of the applied voltage phases on the forward and backward harmonic waves amplitudes for $y = 0.1\ mm$. Conditions: $V_0 = 1\ kV$, $f = 50\ Hz$.

Figure 14. Effect of the number of the dielectric constant of the dielectric barrier on the forward and backward harmonic waves amplitudes for $y = 0.1\,mm$. Conditions: $V_0 = 1\,kV$, $f = 50\,Hz$, 4-phase configuration.

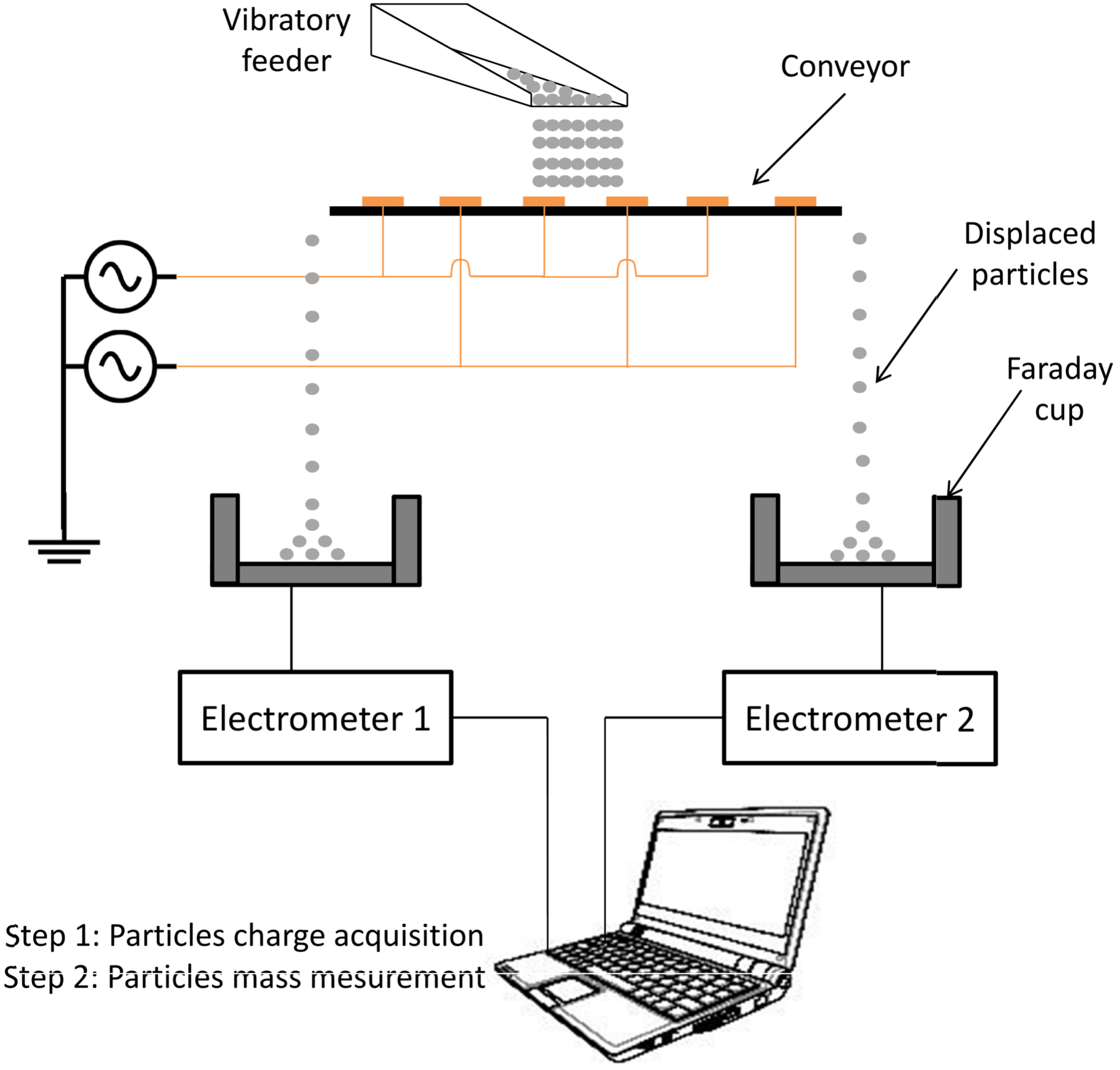
Vibratory feeder
Conveyor
Displaced particles
Faraday cup
Electrometer 1
Electrometer 2
Step 1: Particles charge acquisition
Step 2: Particles mass mesurement

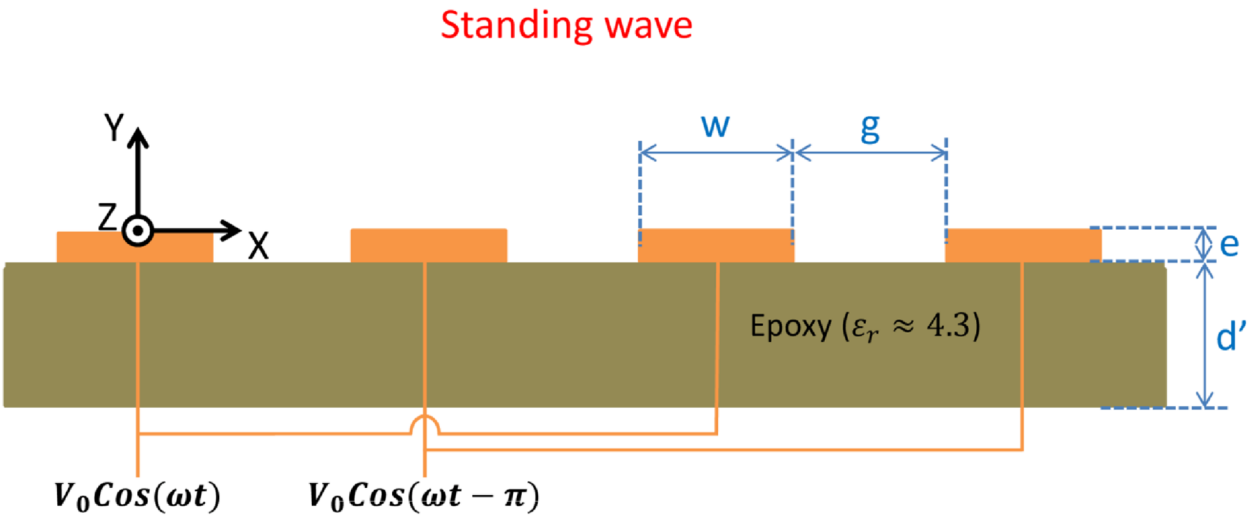
Standing wave
Y
Z
X
w
g
e
d'
Epoxy ($\varepsilon_r \approx 4.3$)
$V_0 Cos(\omega t)$
$V_0 Cos(\omega t - \pi)$

(a) SWC

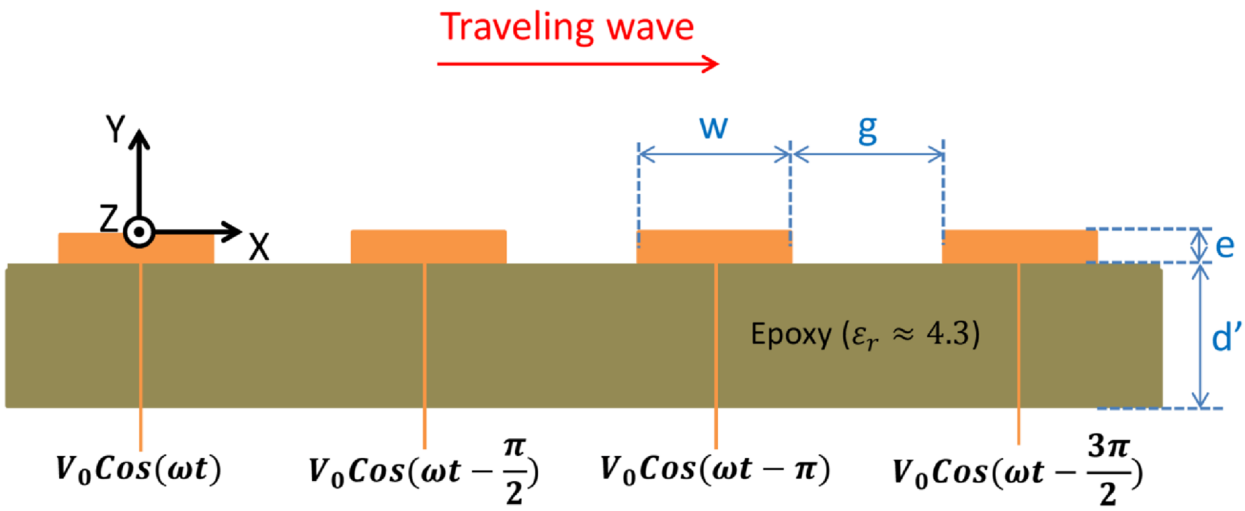
Traveling wave
Y
Z
X
w
g
e
d'
Epoxy ($\varepsilon_r \approx 4.3$)
$V_0 Cos(\omega t)$
$V_0 Cos(\omega t - \frac{\pi}{2})$
$V_0 Cos(\omega t - \pi)$
$V_0 Cos(\omega t - \frac{3\pi}{2})$

(b) TWC

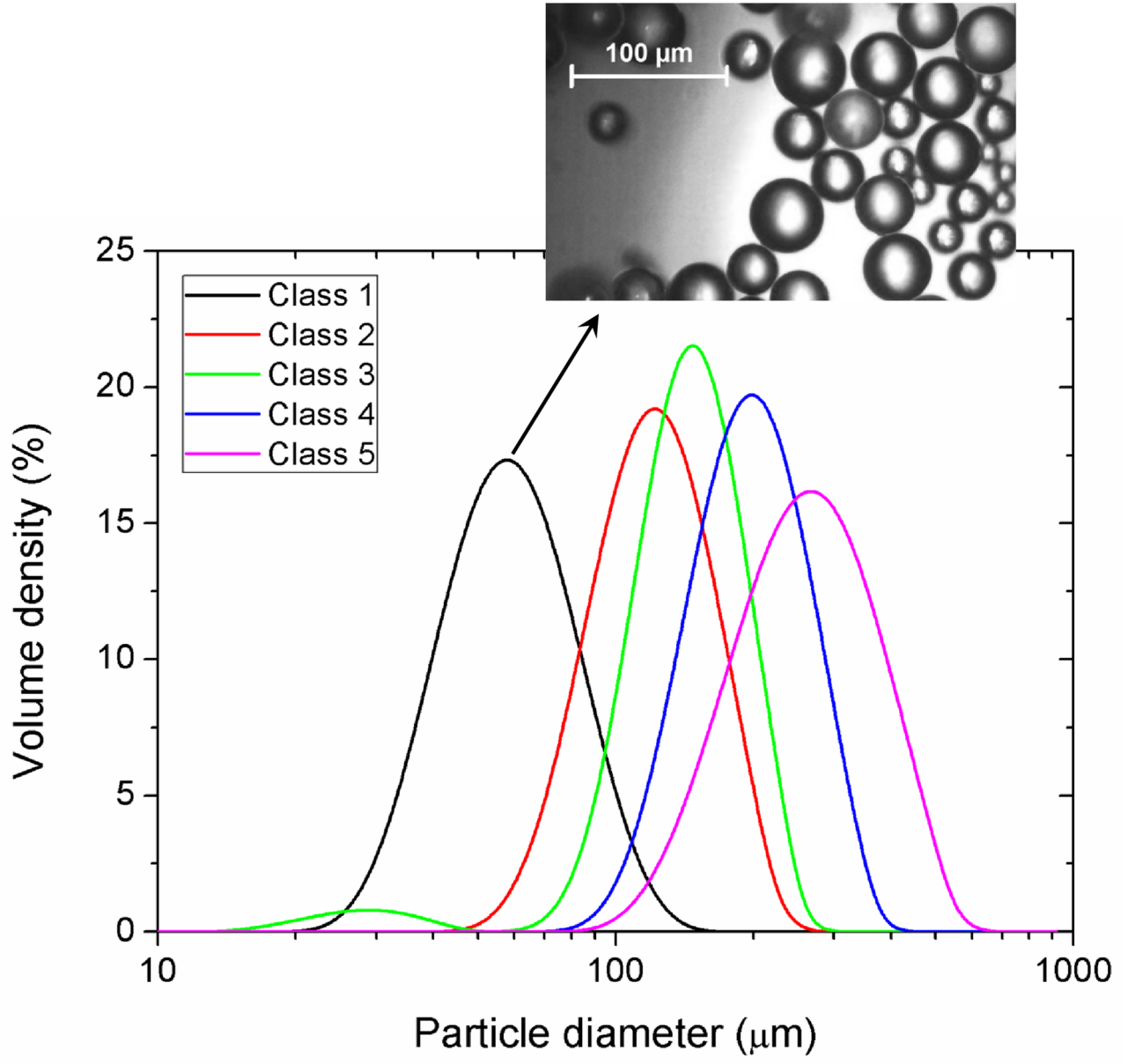
100 µm
Class 1
Class 2
Class 3
Class 4
Class 5
Volume density (%)
Particle diameter (µm)
0
5
10
15
20
25
10
100
1000

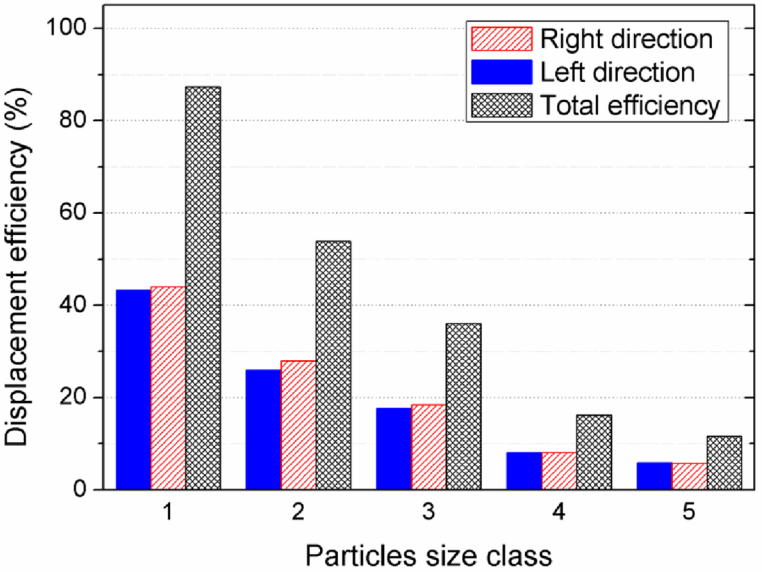
Right direction
Left direction
Total efficiency
Displacement efficiency (%)
0
20
40
60
80
100
1
2
3
4
5
Particles size class

(a) SWC

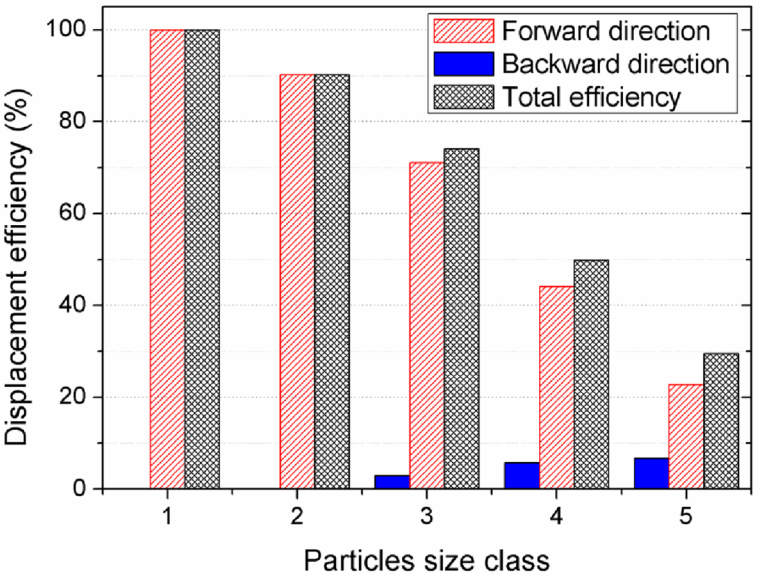
Forward direction
Backward direction
Total efficiency
Displacement efficiency (%)
0
20
40
60
80
100
1
2
3
4
5
Particles size class

(b) TWC

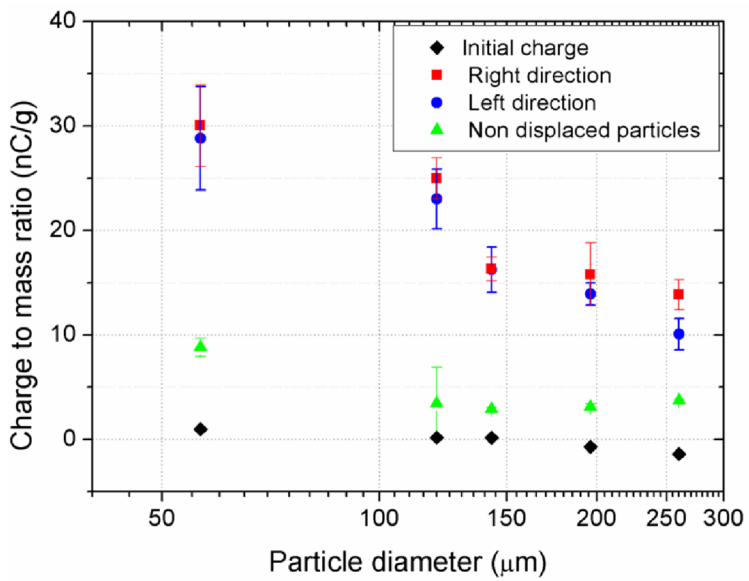
Initial charge
Right direction
Left direction
Non displaced particles
Charge to mass ratio (nC/g)
Particle diameter (μm)
40
30
20
10
0
50
100
150
200
250
300

(a) SWC

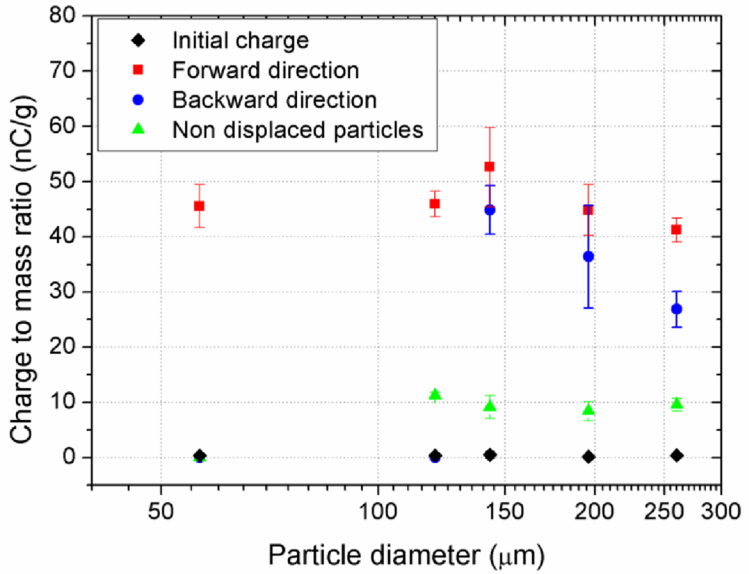
Initial charge
Forward direction
Backward direction
Non displaced particles
Charge to mass ratio (nC/g)
Particle diameter (μm)
80
70
60
50
40
30
20
10
0
50
100
150
200
250
300

(b) TWC

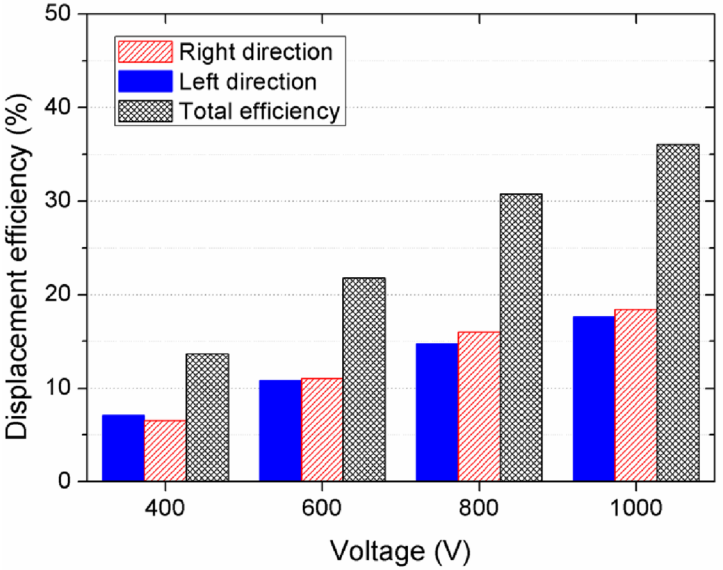
Right direction
Left direction
Total efficiency
Displacement efficiency (%)
0
10
20
30
40
50
400
600
800
1000
Voltage (V)

(a) SWC

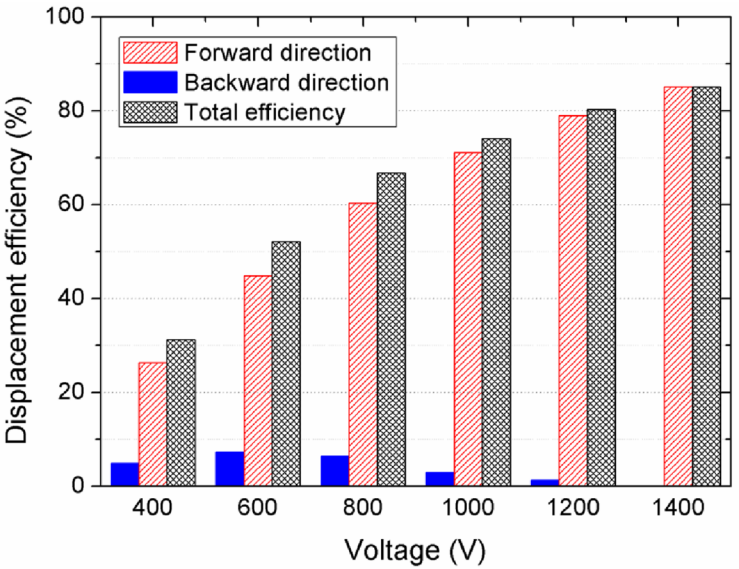
Forward direction
Backward direction
Total efficiency
Displacement efficiency (%)
0
20
40
60
80
100
400
600
800
1000
1200
1400
Voltage (V)

(b) TWC

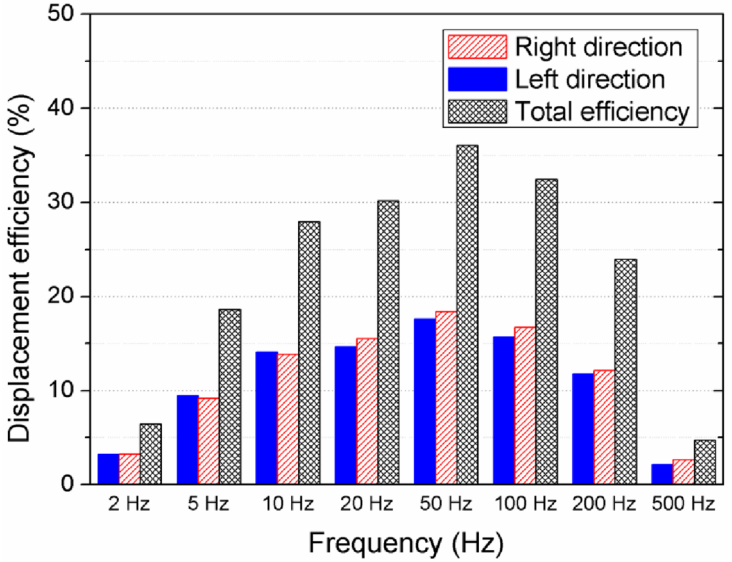
Right direction
Left direction
Total efficiency
Displacement efficiency (%)
0
10
20
30
40
50
2 Hz
5 Hz
10 Hz
20 Hz
50 Hz
100 Hz
200 Hz
500 Hz
Frequency (Hz)

(a) SWC

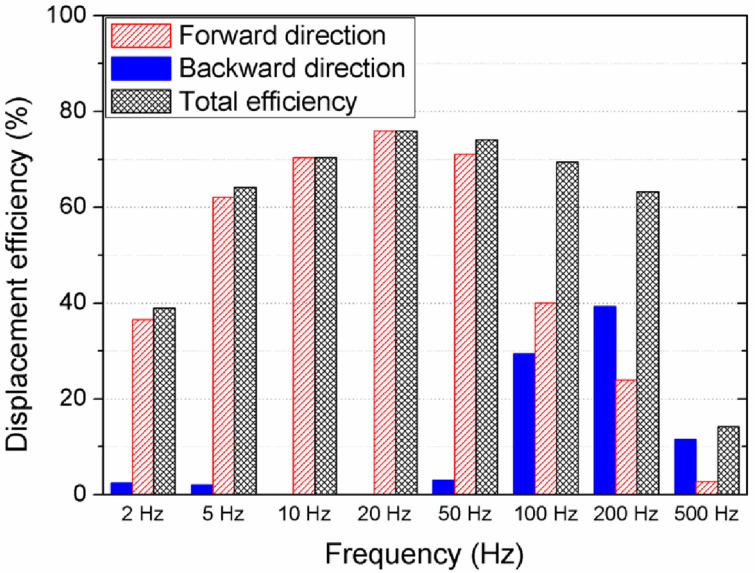
Forward direction
Backward direction
Total efficiency
Displacement efficiency (%)
0
20
40
60
80
100
2 Hz
5 Hz
10 Hz
20 Hz
50 Hz
100 Hz
200 Hz
500 Hz
Frequency (Hz)

(b) TWC

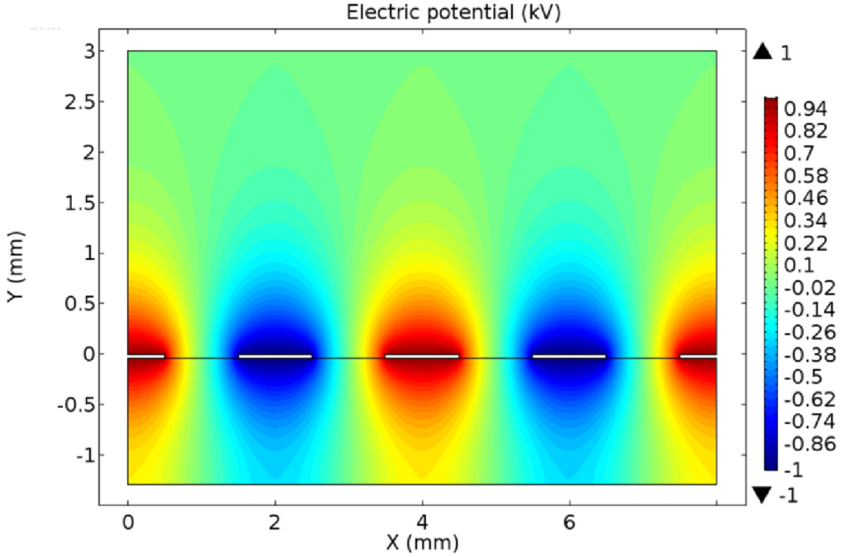
Electric potential (kV)
Y (mm)
X (mm)
3
2.5
2
1.5
1
0.5
0
-0.5
-1
0
2
4
6
▲ 1
0.94
0.82
0.7
0.58
0.46
0.34
0.22
0.1
-0.02
-0.14
-0.26
-0.38
-0.5
-0.62
-0.74
-0.86
-1
▼ -1

(a) SWC

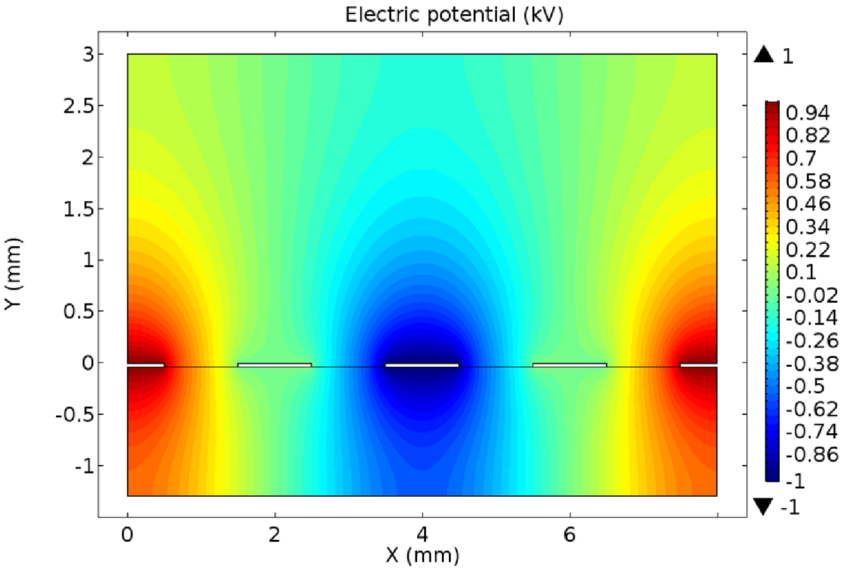
Electric potential (kV)
Y (mm)
X (mm)
3
2.5
2
1.5
1
0.5
0
-0.5
-1
0
2
4
6
▲ 1
0.94
0.82
0.7
0.58
0.46
0.34
0.22
0.1
-0.02
-0.14
-0.26
-0.38
-0.5
-0.62
-0.74
-0.86
-1
▼ -1

(b) TWC

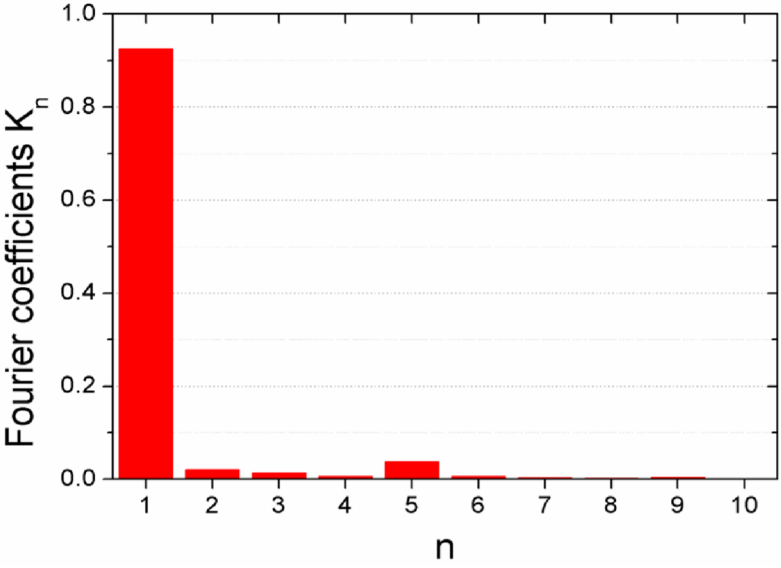
Fourier coefficients K_n
1.0
0.8
0.6
0.4
0.2
0.0
1
2
3
4
5
6
7
8
9
10
n

(a) SWC

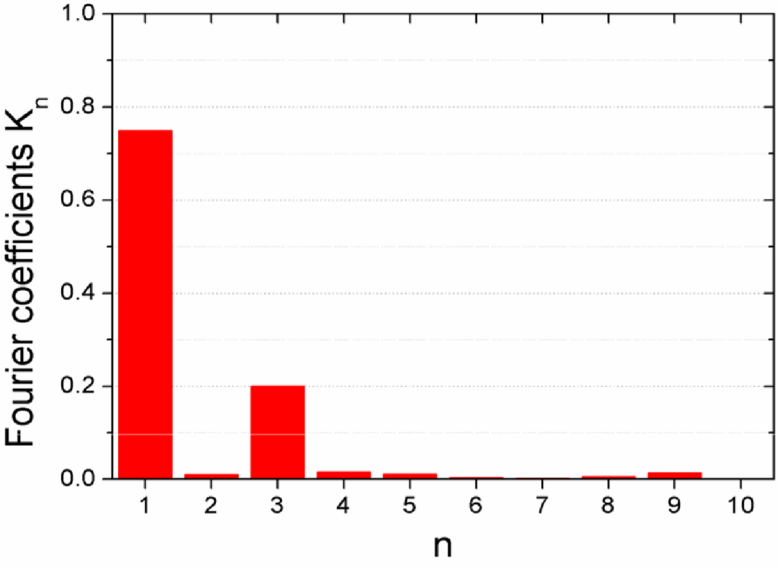
Fourier coefficients K_n
1.0
0.8
0.6
0.4
0.2
0.0
1
2
3
4
5
6
7
8
9
10
n

(b) TWC

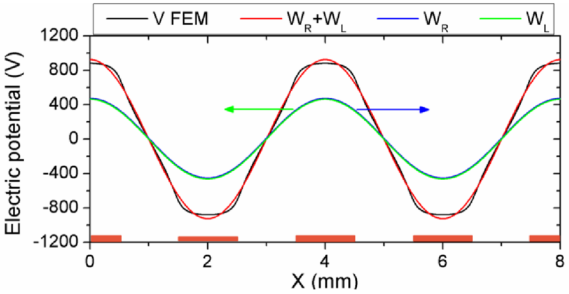

(a) SWC: $t = 0$

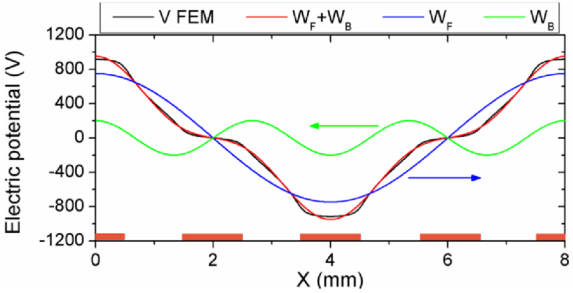

(b) TWC: $t = 0$

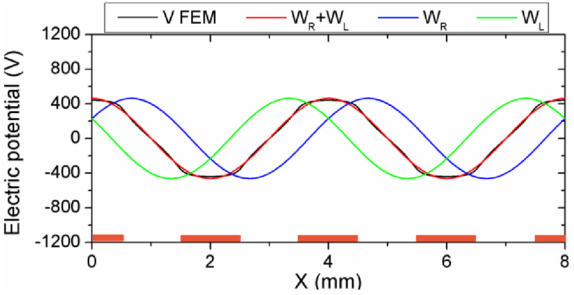

(c) SWC: $t = T / 6$

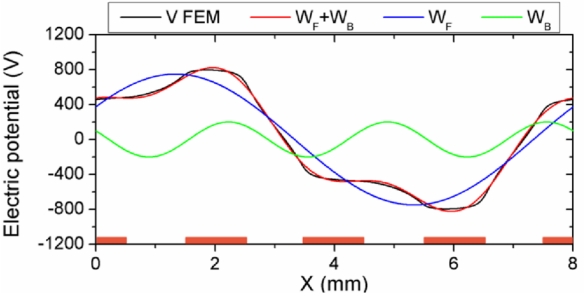

(d) TWC: $t = T / 6$

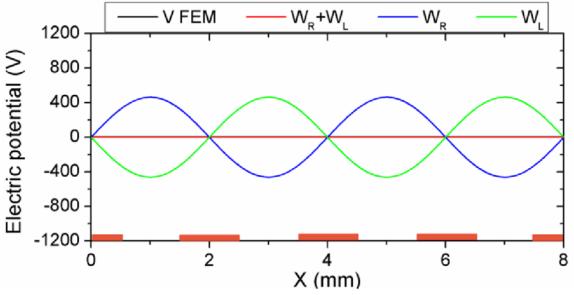

(e) SWC: $t = T / 4$

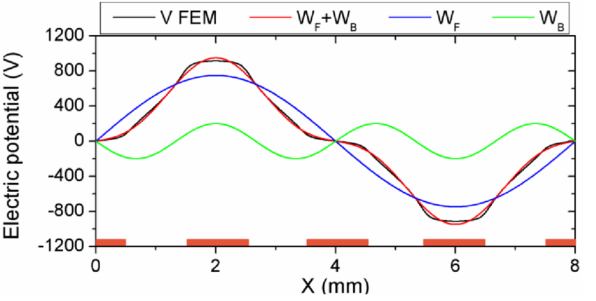

(f) TWC: $t = T / 4$

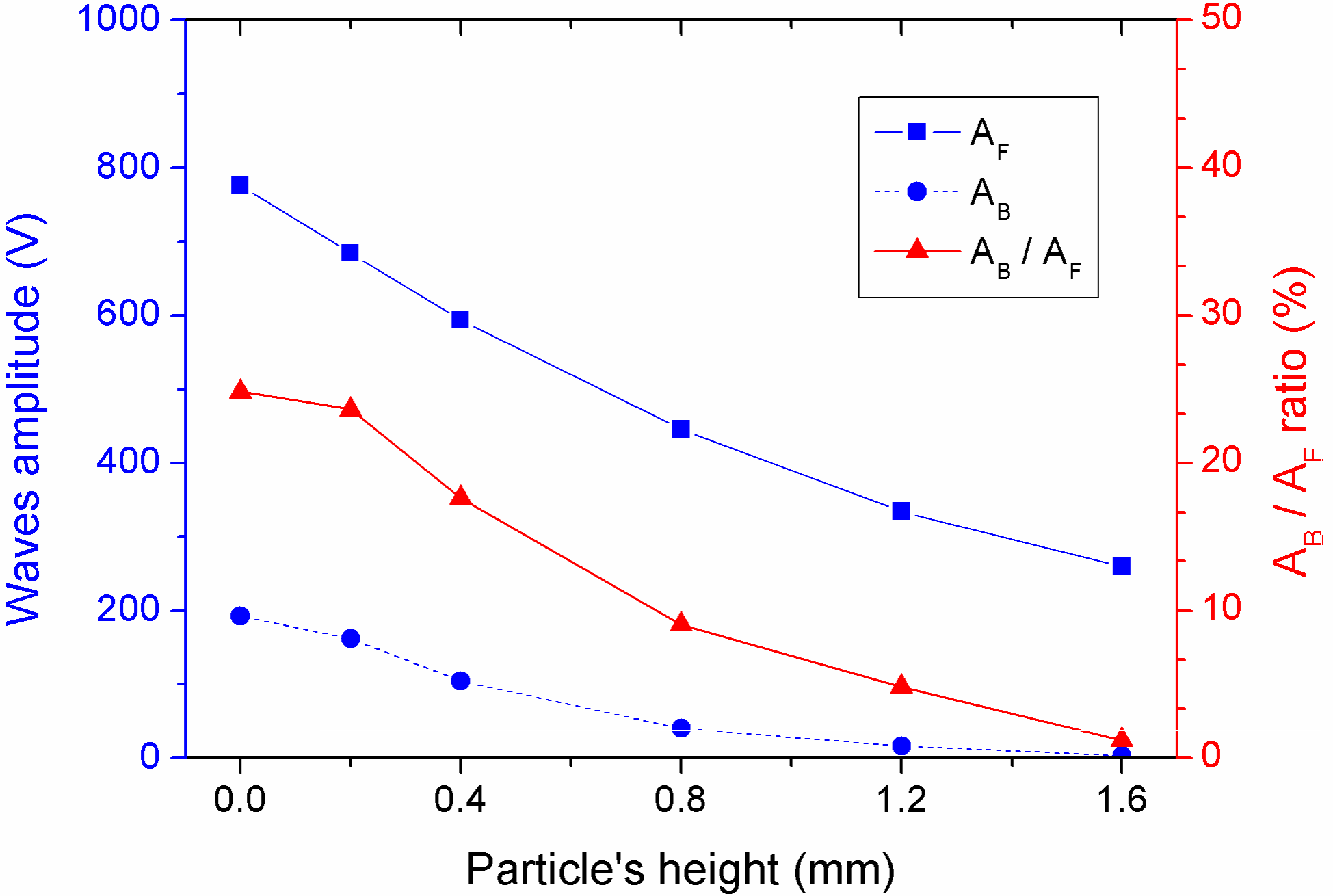
1000
800
600
400
200
0
Waves amplitude (V)
50
40
30
20
10
0
A_B / A_F ratio (%)
0.0
0.4
0.8
1.2
1.6
Particle's height (mm)
A_F
A_B
A_B / A_F

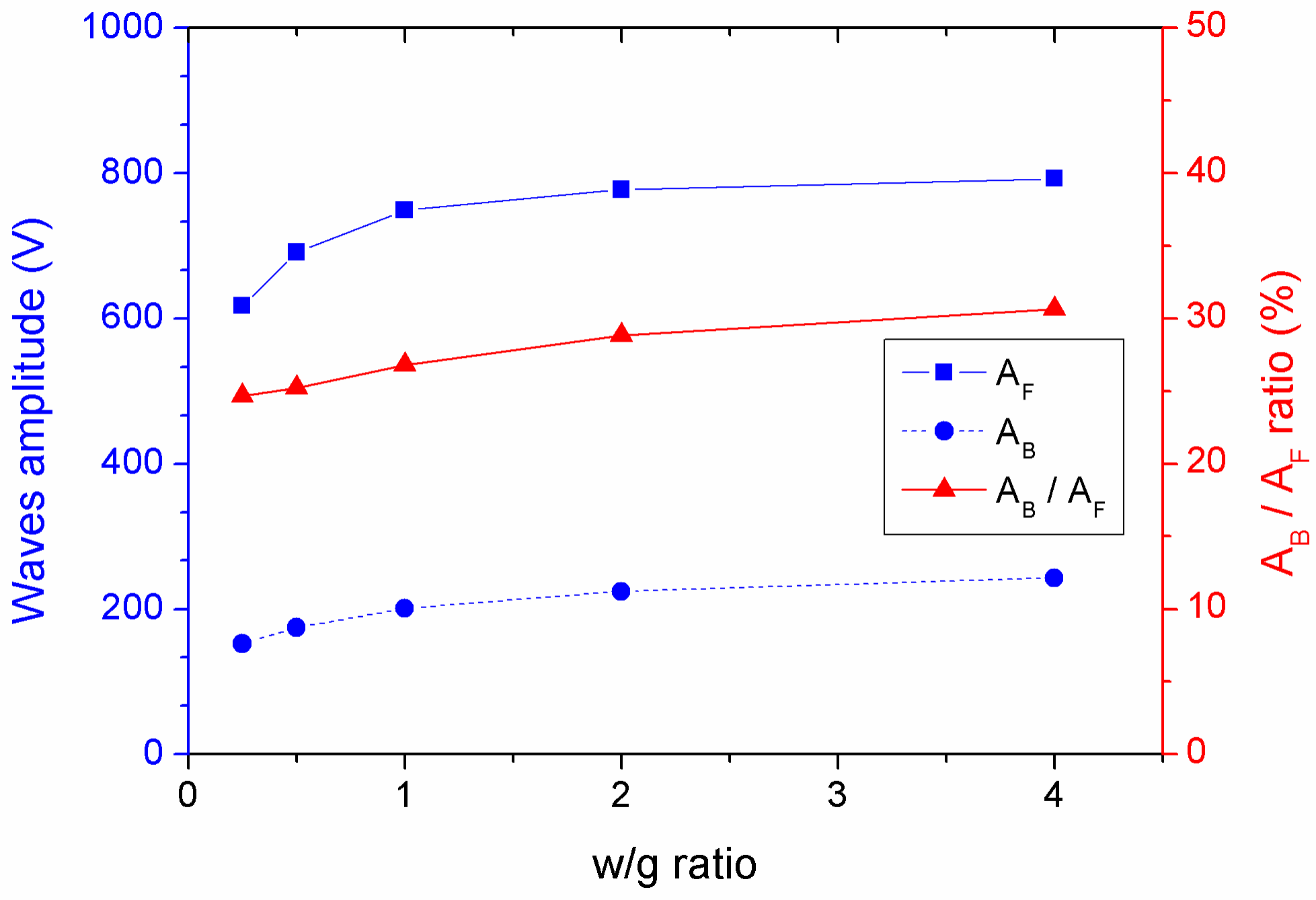
1000
800
600
400
200
0
Waves amplitude (V)
50
40
30
20
10
0
A_B / A_F ratio (%)
0
1
2
3
4
w/g ratio
A_F
A_B
A_B / A_F

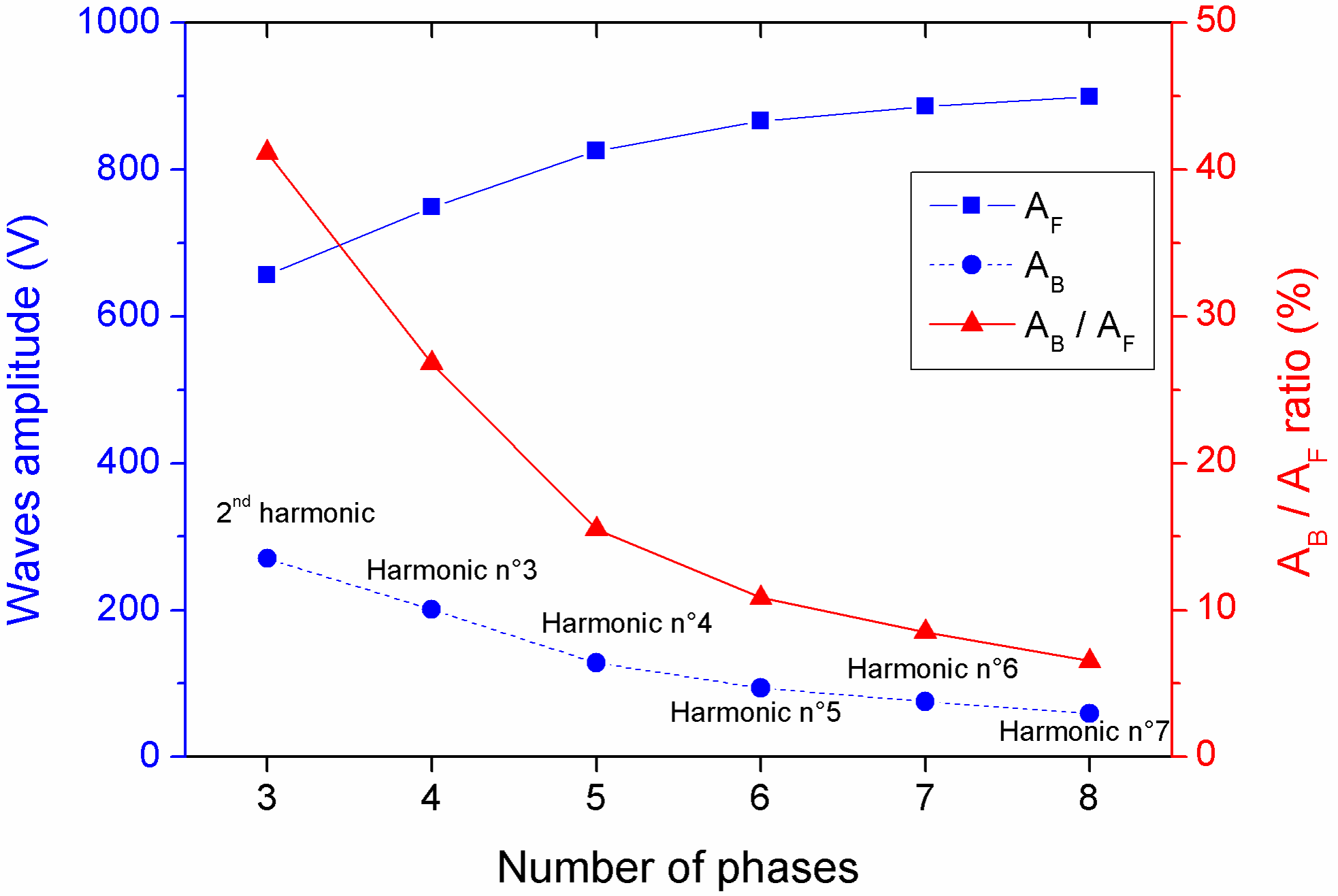
Waves amplitude (V)
A_B / A_F ratio (%)
Number of phases
A_F
A_B
A_B / A_F
2nd harmonic
Harmonic n°3
Harmonic n°4
Harmonic n°5
Harmonic n°6
Harmonic n°7
0
200
400
600
800
1000
0
10
20
30
40
50
3
4
5
6
7
8

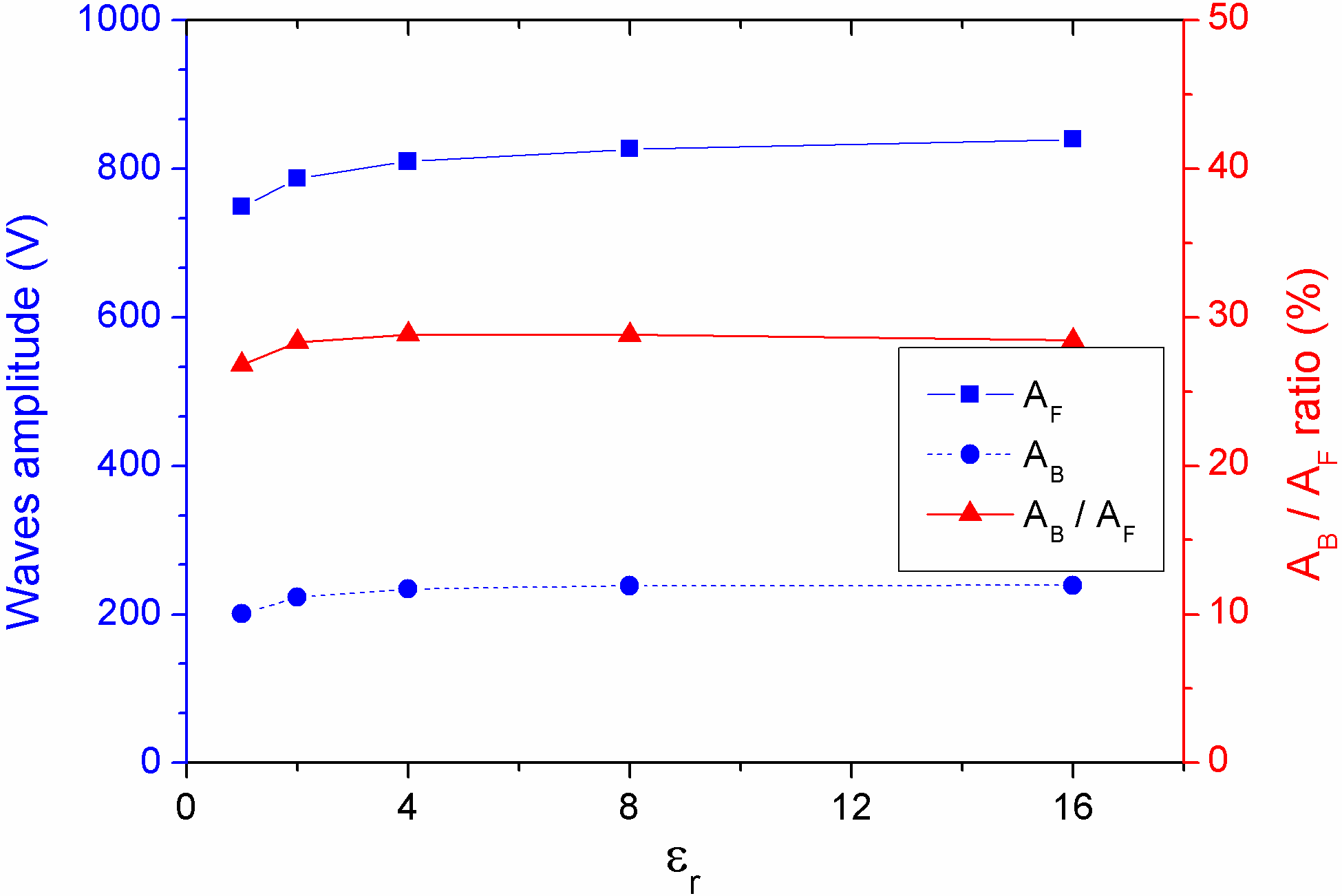
1000
800
600
400
200
0
Waves amplitude (V)
50
40
30
20
10
0
A_B / A_F ratio (%)
0
4
8
12
16
ε_r
A_F
A_B
A_B / A_F